The quasi-one-dimensional character of spin waves in $K_2Fe_7Se_8$

2013 New J. Phys. 15 093043

(http://iopscience.iop.org/1367-2630/15/9/093043)

New Journal of Physics
The open access journal for physics

The quasi-one-dimensional character of spin waves in $K_2Fe_7Se_8$

Feng Lu[1,2], Da-Yong Liu[3], Wei-Hua Wang[1,4], Hui Liu[1] and Weichao Wang[1]

[1] Department of Electronics and Tianjin Key Laboratory of Photo-Electronic Thin film Device and Technology, Nankai University, Tianjin, People's Republic of China
[2] Department of Physics, and Center of Theoretical and Computational Physics, The University of Hong Kong, Hong Kong, People's Republic of China
[3] Key Laboratory of Materials Physics, Institute of Solid State Physics, Chinese Academy of Sciences, Hefei, People's Republic of China
E-mail: whwangnk@nankai.edu.cn

New Journal of Physics **15** (2013) 093043 (9pp)
Received 28 May 2013
Published 30 September 2013
Online at http://www.njp.org/
doi:10.1088/1367-2630/15/9/093043

Abstract. The ground state phase diagram, the physical properties of spin waves and the dynamic structure factor of the new family of 122 iron-vacancy ordered compound $K_2Fe_7Se_8$ are theoretically investigated based on the J_1–J_2 Heisenberg model. Four antiferromagnetic phases are found to be stable in the reasonable physical parameter region. The dispersion relations of the spin waves for the newly discovered AFM2 and AFM3 phases are studied using the linearized spin wave theory. Two acoustic spin wave branches and 12 optical spin wave branches are present in both the AFM2 and AFM3 phases, and each of them are twofold degenerate. One more interesting finding is that the spin waves of $K_2Fe_7Se_8$ have the quasi-one-dimensional character at the high frequency range. To offer theoretical guidance for the further neutron scattering experiments, the inelastic neutron scattering patterns for the AFM2 and AFM3 phases are also investigated.

[4] Author to whom any correspondence should be addressed.

Contents

1. Introduction

Over the past five years, searching for high transition temperature (T_c) superconductors in iron-based pnictides [1–8] has been one of the central topics in condensed matter physics, since the discovery of the second class of high T_c superconductors in LaFeAsO [1]. Many iron-based compounds were reported to show superconductivity after doping or under high pressures, such as ReFeAsO (1111 crystal structure) [1, 4], AFe_2As_2 (A = Ca, Ba) (122 crystal structure) [5, 6], LiFeAs (111 crystal structure) [8] and FeSe (11 crystal structure) [7]. Recently, the discovery of the new family AFe_2Se_2 (A = K, Rb or Tl) superconductors with iron vacancy-ordered has stimulated great interest in the study of iron pnictides with 122 crystal structure [9–12]. For example, $A_yFe_{2-x}Se_2$ (A = K, Rb or Tl) have been found to become superconducting at about 30 K [9–11]. The AFe_2Se_2 compounds have the same $ThCr_2Si_2$-type crystal structure as that of the 122 compounds. However, there are many unique physical properties for the AFe_2Se_2 compounds, which are different from those of the iron-based superconductors with the similar crystal structure, such as the absence of the hole-like Fermi surface in $K_{0.8}Fe_{1.7}Se_2$ [13], the block antiferromagnetic (AFM) order in $K_{0.8}Fe_{1.6}Se_2$ [14], and the intrinsic $\sqrt{5} \times \sqrt{5}$ iron vacancies superstructure in $K_{0.8}Fe_{1.6}Se_2$ [15].

To date, numerous research has been carried out to study the nature of iron vacancy-ordered compounds [14, 15]. Different from the random iron vacancies, the ordered iron vacancies cause the $A_yFe_{2-x}Se_2$ (A = K, Rb or Tl) have a new supercell structure, inducing the interesting electronic structure [14] and magnetic ground states [14, 15]. Since $A_yFe_{2-x}Se_2$ shows superconductivity by doping with hole [9–12], one of the important questions is 'what is the actual parent phase of these superconductors?' [16, 17]. The $A_2Fe_4Se_5$ compound has been suggested as the parent compound [14, 15] and the Cooper pairs were mediated by the AFM spin fluctuation [14, 15, 18]. Recently, a novel ordered iron vacancy compound $A_2Fe_7Se_8$ has been discovered by a scanning tunneling microscopy experiment [17], which was proposed to be the parent phase. Each iron vacancy exists in every eight iron sites, so $A_2Fe_7Se_8$ has the intrinsic $\sqrt{8} \times \sqrt{10}$ iron vacancies structure. As we know, the magnetic configurations and the relevant physical properties are very important in superconductors. However, until recently, research about the magnetic ground state and the magnetic properties for $A_2Fe_7Se_8$ materials was still scarce. Thus, it is critical to study the magnetic ground state and spin waves of $A_2Fe_7Se_8$ for a better understanding of the physical mechanism of its superconductivity.

To give a qualitative insight into the magnetic ground state and spin wave properties in this system, we have investigated the magnetic ground state phase diagram, as well as the spin waves of $K_2Fe_7Se_8$. Based on our results, four AFM phases are found to be stable in the reasonable parameter region, such as the conventional collinear AFM and three newly discovered

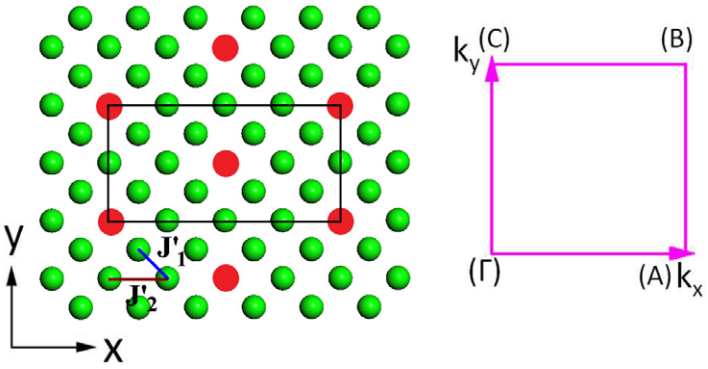

Figure 1. Schematic diagram of the two-dimensional crystal structure of $K_2Fe_7Se_8$ and the corresponding Brillouin zone (BZ). Left side is the crystal structure of $K_2Fe_7Se_8$. The black solid line marks the magnetic unit cell. The iron vacancy site Fe is marked by the red circle, and the occupied site Fe is marked by the green circle. Right side is the BZ of the magnetic unit cell. In the following, the spin waves are plotted along the highly symmetric direction Γ–A–B–Γ–C–A.

AFM phases. Using the linear spin wave theory, we have investigated the dispersion relations of the spin wave for the newly discovered AFM2 and AFM3 phases, which have two acoustic spin wave branches and 12 optical spin wave branches. Along with the special directions, the spin system displays the quasi-one-dimensional character at high frequency. To compare with future neutron scattering experiments, the inelastic neutron scattering patterns for the AFM2 and AFM3 phases are also calculated and discussed. The rest of this paper is organized as follows. In section 2, the theoretical model and calculation details are described; in section 3, the phase diagram, spin waves and dynamical structure factor for the newly discovered AFM2 and AFM3 phases are investigated, respectively. The last part is devoted to the conclusion.

2. Model and method

One of the minimal theoretical model for $K_2Fe_7Se_8$ is the J_1–J_2 Heisenberg model on a quasi-two-dimensional lattice, which can capture the essential physics of the magnetism in this Fe-vacancies ordered materials [19]

$$H = J_{\mathrm{NN}} \sum_{i,\delta} \mathbf{S}_i \cdot \mathbf{S}_{i+\delta} + J_{\mathrm{NNN}} \sum_{i,\delta'} \mathbf{S}_i \cdot \mathbf{S}_{i+\delta'}, \tag{1}$$

where δ and δ' represent the nearest-neighbor (NN) and next nearest-neighbor (NNN) site of the ith site, respectively. The first term denotes the NN spin interaction and the corresponding coupling constant is J_{NN}. The spin interaction between the NNN is described by the second term and J_{NNN} is the corresponding coupling constant. In the following, the J_{NN} and J_{NNN} near Fe vacancies are expressed by J_1' and J_2' respectively, as shown in figure 1; other spin coupling constants J_{NN} and J_{NNN} are expressed by J_1 and J_2, respectively. For convenience, we define $|J_1|S$ as the energy unit. The scanning tunneling microscopy experiment suggests that $K_2Fe_7Se_8$ has the $\sqrt{8} \times \sqrt{10}$ Fe-vacancies ordered structure [17]. Therefore, each magnetic unit cell contains two crystal unit cells for the AFM configuration in figure 1, which includes

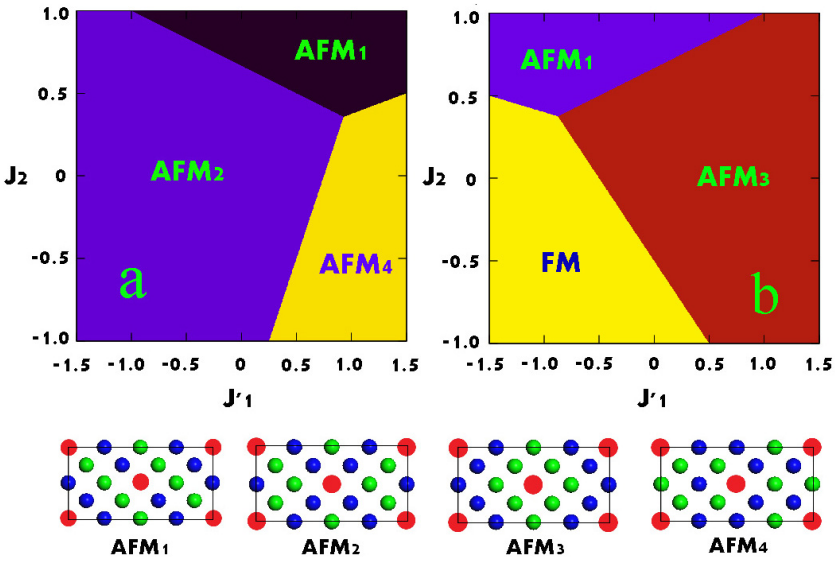

Figure 2. The phase diagram for the $J_1(J_1') - J_2(J_2')$ Heisenberg model. The blue and green atoms indicate the Fe-atoms with positive and negative magnetic moment, respectively. (a) The phase diagram for the interaction parameter $J_1 = 1$, $J_2' = 1$. (b) The phase diagram for the interaction parameter $J_1 = -1$, $J_2' = 1$. AFM1, AFM2, AFM3 and AFM4 represent the antiferromagnetic order, and FM represents ferromagnetic order.

14 iron atoms and 2 iron vacancies. The two-dimensional Brillouin zone (BZ) and the high symmetry points are also shown in figure 1.

We use Holstein–Primakoff (HP) transformations to investigate the spin waves of the AFM2 and AFM3 phases, which is a standard procedure to calculate the spin wave [20–22]. Under HP transformations, we can obtain the HP boson Hamiltonian

$$H = \sum_k \psi_k^\dagger \mathcal{H}_k \psi_k + E_0 - N E_{(k=0)}. \tag{2}$$

Here, $\psi_k^\dagger$ is the boson operators, $\psi_k^\dagger = (a_{k1}^\dagger \ldots a_{k7}^\dagger b_{-k-1} \ldots b_{-k-7})$, which is determined by the magnetic ground state. E_0 is the constant for the classical ground state energy. We can obtain the dispersion relations of the spin wave by the standard numerical diagonalization method [23].

3. Results and discussions

The mean-field approximation is used to investigate the ground state magnetic structure of the J_1–J_2 Heisenberg model on a quasi-two-dimensional lattice. In the present study, the ferromagnetic (FM) and all the collinear AFM structures are taken into account, and the non-collinear magnetic structure is not considered. The magnetic phase diagram of $K_2Fe_7Se_8$ is shown in figure 2. Owing to four different parameters in the J_1–J_2 Heisenberg model, the phase diagram is plotted in the $J_1' - J_2$ space while other parameters are fixed, i.e. $J_1 = \pm 1$ and $J_2' = 1$. There are three phases in the $J_1' - J_2$ space for the case $J_1 = 1$: the collinear AFM1, AFM2 and AFM3 phases, as shown in figure 2(a). Actually, the collinear AFM1 phase is one of the stable phases for both the case $J_1 = 1$ and the case $J_1 = -1$, as discussed below. Besides the

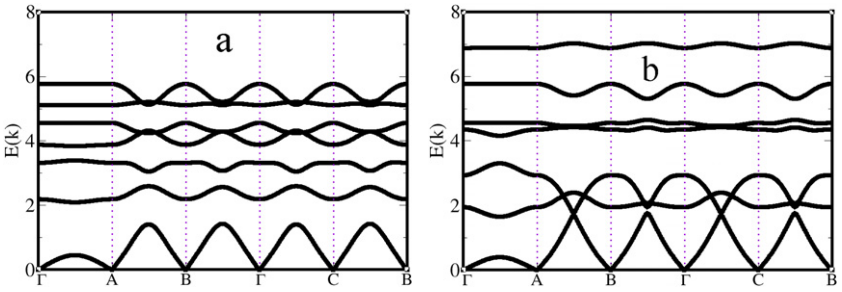

Figure 3. The spin waves as a function of k along selected high symmetry directions in the magnetic unit cell BZ. (a) The spin waves for AFM2 phase. (b) The spin waves for AFM3 phase.

AFM1 phase, there are two newly discovered stable AFM phases for the case $J_1 = 1$: AFM2 and AFM4. As we know, the AFM1 phase is a popular magnetic configuration, which has been much studied [12, 24]. Thus, we focus on the newly discovered AFM phases in this paper, which only appear in the $\sqrt{8} \times \sqrt{10}$ iron vacancies structure. In the AFM2 configuration, a 'super-moment' occurs in the situation of the six positive spins along the diagonal direction around the centered Fe vacancy and another opposite spin located in the left and right boundary of the supercell. The super-moment forms a simple Neel AFM order on a square lattice, as seen from figure 2. It is easy to understand this magnetic configuration from the J_1–J_2 model. When the spin coupling J_1' is dominant in the parameter region (i.e. $J_1' \to -\infty$), J_1' favors the FM magnetic configuration along the diagonal direction around the centered Fe vacancy, which induces the super-moment. The Neel AFM configuration between the different super-moments is induced by other spin interactions. Thus, the AFM2 phase emerges in this parameter region. The other newly discovered AFM4 phase in figure 2 has a much lower symmetry, which is different from the AFM1 and AFM2 phases.

When $J_1 = -1$, the AFM1 phase also appears in the phase diagram of figure 2(b). Remarkably, the FM phase is robust in a large parameter space especially in the region $J_{\mathrm{NN}} < 0$ and $J_{\mathrm{NNN}} < 0$, because the negative exchange couplings lead to the FM alignment of Fe spins. Noticeably, the AFM3 is the only robust AFM phase at $J_1 = -1$. It can be regarded as seven parallel spins around the centered Fe vacancy and all the other spins have the antiparallel direction in the super cell.

To give a qualitatively understanding of the newly discovered AFM2 and AFM3 phases, we will discuss their spin wave characters based on the linear spin wave theory. The linear spin wave theory is good enough to capture the main properties of the spin wave [25, 26]. But if one wants to obtain more details about the spin wave, the second order perturbation theory [27–30], self-consistent spin wave theory [31–34] or coupled-cluster calculations [35–37] can be employed. As we discussed above, due to the 14 sites in the magnetic unit cell, it is very hard to obtain the explicitly analytical expressions for the spin wave dispersion relations. Thus the spin wave can be calculated by the numerical diagonalization method [23]. The spin wave dispersion relations of the AFM2 and AFM3 phases along the high symmetry directions are shown in figure 3. For convenience, a set of typical parameters ($J_1 = 1$, $J_1' = -0.8$, $J_2 = -0.6$, $J_2' = 1$) for AFM2 phase and ($J_1 = -1$, $J_1' = 0.8$, $J_2 = -0.6$, $J_2' = 1$) AFM3 phase are chosen in the numerical calculation. As shown in figure 1, there are 16 sites in the magnetic unit cell. However, the number of spin waves

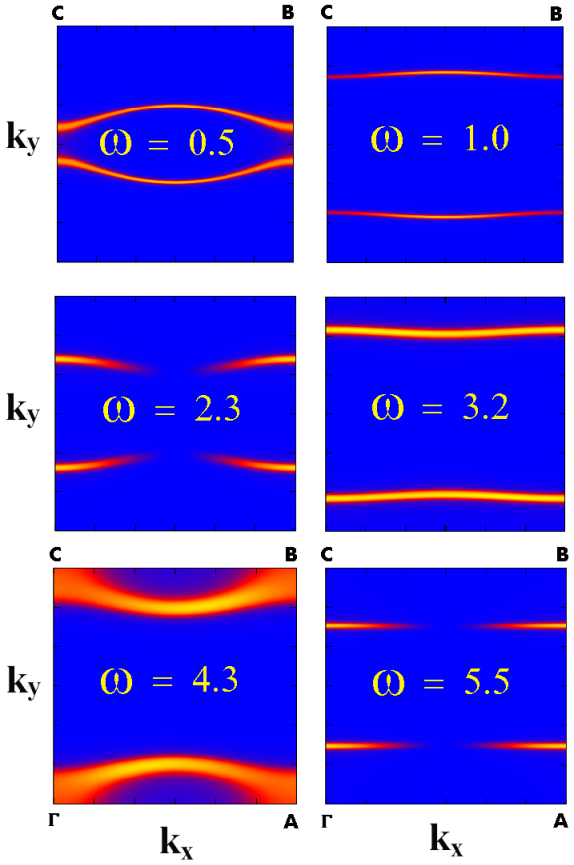

Figure 4. Constant-energy cuts (untwinned) of the dynamic structure factor $S^{\text{in}}(k, \omega)$ for AFM2 phase. The x-axis and y-axis correspond to k_x (Γ–A) and k_y (Γ–C) directions in the BZ of the magnetic unit cell, as shown in figure 1. The frequency ω is in units of $|J_1|$. The color indicates the intensity of diffraction peaks. The brighter of the color, the stronger of the intensity of diffraction peaks. The theoretical parameters are the same as that in figure 3.

is decided by the number of iron atoms in the magnetic unit cell. Hence, 14 spin wave branches are generated in the AFM2 phase, including 2 acoustic spin wave branches and 12 optical spin wave branches. Each of the spin waves has twofold degeneracy, since the system holds invariance under the translational operation of $T(1/2\vec{x} + 1/2\vec{y})$ and reversion of spins I_-. From Goldstone's theorem, the acoustic branches do not have a gap at the Γ point, which corresponds to a kind of collective excitation mode involving all the 14 spin sites. All 12 optical spin wave branches have gaps at the Γ point and the gaps are dependent on the specific interaction parameters. Along the high symmetry directions of Γ–A and C–B at higher frequencies, all the spin wave dispersions are very weak, which indicates the quasi-one-dimensional character in this system. The quasi-one-dimensional character of spin waves can be attributed to the existence of the iron vacancy along the x direction. In contrast, all the spin waves along other high symmetry directions have obvious dispersions, which can be clearly seen in figure 3(a). For the AFM3 phase, there are also 2 acoustic spin wave branches and 12 optical spin wave branches, and each of the spin waves is also twofold degenerate due to the same symmetry. The corresponding spin wave has a similar dispersion to that of the

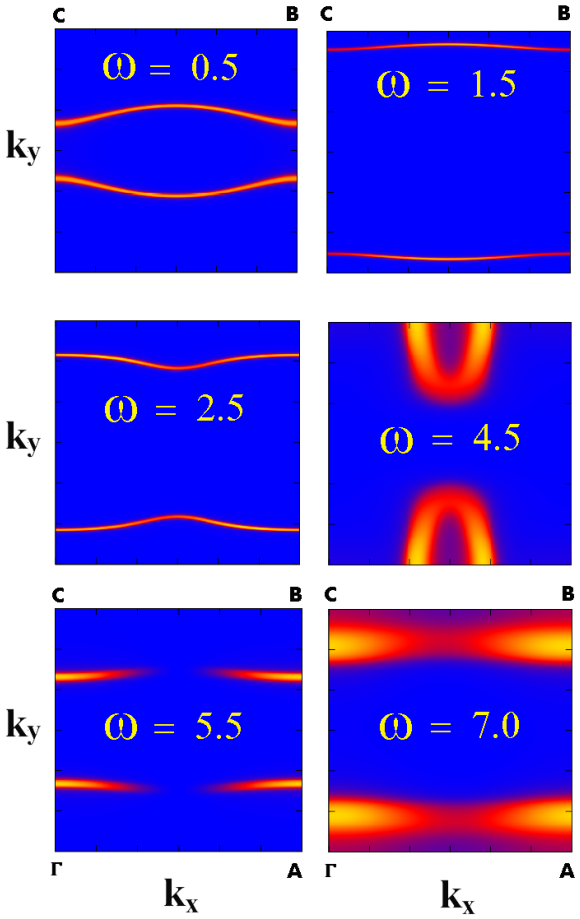

Figure 5. Constant-energy cuts (untwinned) of the dynamic structure factor $S^{\text{in}}(k, \omega)$ for AFM3 phase. The x-axis and y-axis correspond to $k_x(\Gamma{-}A)$ and $k_y(\Gamma{-}C)$ directions of the BZ of the magnetic unit cell, as shown in figure 1. The frequency ω is in units of $|J_1|$. Similar to figure 4, the color indicates the intensity of diffraction peaks. The theoretical parameters are the same to those in figure 3.

AFM2 phase. Moreover, the quasi-one-dimensional character along the $\Gamma{-}A$ direction also appears at high frequency. The quasi-one-dimensional spin wave character can be measured by the inelastic neutron scattering experiment. To provide some insights for further neutron scattering experiments, we investigate the expected neutron scattering intensity at different constant frequency cuts in k-space, which is proportional to the dynamic structure factor $S^{\text{in}}(k, \omega)$. The zero-temperature dynamic structure factor can be calculated by HP bosons. In the linear spin wave approximation, only S^x_k and S^y_k contribute to the inelastic neutron scattering intensity through single magnon excitations and S^z_k only contributes to the elastic part of the neutron scattering intensity. The spin dynamical factor associated with the spin-waves is given [19, 21–23],

$$S^{\text{in}}(k, \omega) = S \sum_f |\langle f| \sum_n \xi_{kn} \alpha_n^\dagger |0\rangle|.$$

Here, $|0\rangle$ denotes the magnon vacuum state, $|f\rangle$ is the final state [21] and ξ_{kn} is the nth component of the eigenvector $\alpha_n^\dagger|0\rangle$.

In the fixed energy cuts, the expected neutron scattering intensity patterns of AFM2 and AFM3 phases are shown in figures 4 and 5, respectively. At the frequency cut $\omega = 0.5$, there are two curves along the k_x direction for the AFM2 phase, resulting from the acoustic spin wave branches, as shown in figure 4. With the increase of the cut frequency to $\omega = 1.0$, the distance between the two curves becomes bigger, which come from the first twofold degeneracy optical spin-wave branches. Different from the low frequency situation, at higher frequency $\omega = 2.3$, the distance of diffraction peaks becomes smaller. Simultaneously, the intensity of diffraction peaks around the Γ point becomes weaker and less obvious. At $\omega = 3.2$, the distance between diffraction peaks becomes much bigger and the intensity of diffraction peaks at the $k_x = 0$ point becomes stronger due to the contribution of the second twofold degeneracy optical spin-wave branches. At frequency cut $\omega = 4.3$, the diffraction peaks appear in the corner of the BZ and become broader due to the third and fourth twofold degeneracy optical spin-wave branches. At the highest frequency $\omega = 5.5$, the diffraction peaks become narrower and fainter. At the same time, the middle diffraction peaks around the Γ point become very weak and vanish again due to the contribution of the fifth and sixth twofold degeneracy optical spin-wave branches.

As shown in figure 5, the diffraction peaks for the AFM3 phase are similar to those of the AFM2 phase. At $\omega = 0.5$, two bright curves exist, originating from the acoustic spin wave branches. At $\omega = 1.5$, the curves of the dynamic structure factor appear at the edge of BZ and become narrower. At the intermediate frequency $\omega = 2.5$, the distance between diffraction peaks becomes smaller and the intensity of diffraction peaks becomes stronger. At higher frequency $\omega = 4.5$, the diffraction peaks become two semi-elliptical shapes near the boundary of BZ due to the contribution of the third and fourth twofold degeneracy optical spin-wave branches. At $\omega = 5.5$, the diffraction peaks move close to $k_y = 0$, and the middle diffraction peaks around the Γ point disappear. In contrast, at the highest frequency $\omega = 7.0$, the diffraction peaks at $k_x = 0$ point appear again and the broad diffraction peaks appear near the boundary of BZ.

4. Conclusions

In conclusion, we have provided a natural and unified understanding of magnetism and vacancy ordering in $K_2Fe_7Se_8$ through investigation of the magnetic ground state phase diagram of the J_1–J_2 model. In the phase diagram, there are three AFM phases in the parameter region $J_1 > 0$ and two AFM phases in the parameter region $J_1 < 0$, which can be applied to understand the possible magnetic ground state of $K_2Fe_7Se_8$. Based on the linearized spin wave theory, we have investigated the spin waves for the AFM2 and AFM3 phases, which can be measured and verified by future neutron scattering experiments. Two acoustic spin wave branches and 12 optical spin wave branches coexist in the AFM2 and AFM3 phases. Moreover, the spin waves of $K_2Fe_7Se_8$ have a quasi-one-dimensional character at high frequencies. To supply some guidance for future neutron scattering experiments, we also calculated the inelastic neutron scattering pattern for the AFM2 and AFM3 phases.

Acknowledgments

The authors thank Professor F C Zhang, Professor C Cao for the fruitful discussions and Mr C Gong for his careful reading and refining of some expressions. This work was supported by the National Natural Science Foundation of China (numbers 11104148 and 11047162), Tianjin Key

Technology R&D Program (number 11ZCKFGX01300), the Research Fund for the Doctoral Program of Higher Education (numbers 20100031120035 and 20110031110034).

References

[1] Kamihara Y, Watanabe T, Hirano M and Hosono H 2008 *J. Am. Chem. Soc.* **130** 3296
[2] Chen G F *et al* 2008 *Phys. Rev. Lett.* **101** 057007
[3] Yang S, You W L, Gu S J and Lin H Q 2009 *Chin. Phys.* B **18** 2545
[4] Haindl S *et al* 2010 *Phys. Rev. Lett.* **104** 077001
[5] Baek S H, Lee H, Brown S E, Curro N J, Bauer E D, Ronning F, Park T and Thompson J D 2009 *Phys. Rev. Lett.* **102** 227601
[6] Chen Z G, Dong T, Ruan R H, Hu B F, Cheng B, Hu W Z, Zheng P, Fang Z, Dai X and Wang N L 2010 *Phys. Rev. Lett.* **105** 097003
[7] Xu Z J, Wen J S, Xu G Y, Jie Q, Lin Z W, Li Q, Chi S X, Singh D K, Gu G and Tranquada J M 2010 *Phys. Rev.* B **82** 104525
[8] Inosov D S *et al* 2010 *Phys. Rev. Lett.* **104** 187001
[9] Guo J G, Jin S F, Wang G, Wang S C, Zhu K X, Zhou T T, He M and Chen X L 2010 *Phys. Rev.* B **82** 180520
[10] Fang M H, Wang H D, Dong C H, Li Z J, Feng C M, Chen J and Yuan H Q 2011 *Europhys. Lett.* **94** 27009
[11] Wang H D, Dong C H, Li Z J, Zhu S S, Mao Q H, Feng C M, Yuan H Q and Fang M H 2011 *Europhys. Lett.* **93** 47004
[12] Yan X-W, Gao M, Lu Z-Y and Xiang T 2011 *Phys. Rev. Lett.* **106** 087005
[13] Qian T *et al* 2011 *Phys. Rev. Lett.* **106** 187001
[14] Cao C and Dai J H 2011 *Phys. Rev. Lett.* **107** 056401
[15] Bao W, Huang Q Z, Chen G F, Green M A, Wang D M, He J B and Qiu Y M 2011 *Chin. Phys. Lett.* **28** 086104
[16] Cao C and Zhang F C 2013 *Phys. Rev.* B **87** 161105
[17] Ding X X, Fang D L, Wang Z Y, Yang H, Liu J Z, Deng Q, Ma G B, Meng C, Hu Y H and Wen H H 2013 *Nature Commun.* **4** 1897
[18] You Y-Z, Yang F, Kou S-P and Weng Z-Y 2011 *Phys. Rev. Lett.* **107** 167001
[19] Lu F and Wang W H 2012 *Phy. Lett.* A **375** 4203
[20] Auerbach A 1994 *Phys. Rev. Lett.* **72** 2931
[21] Carlson E W, Yao D X and Campbell D K 2004 *Phys. Rev.* B **70** 064505
[22] Yao D X, Carlson E W and Campbell D K 2006 *Phys. Rev. Lett.* **97** 017003
[23] Lu F and Dai X 2012 *Chin. Phys.* B **21** 027502
[24] Fang C, Bernevig B A and Hu J P 2009 *Europhys. Lett.* **86** 67005
[25] Wang M Y *et al* 2011 *Nature Commun.* **2** 580
[26] Fang C, Xu B, Dai P C, Xiang T and Hu J P 2012 *Phys. Rev.* B **85** 134406
[27] Igarashi J and Nagao T 2005 *Phys. Rev.* B **72** 014403
[28] Oitmaa J and Hamer C J 2008 *Phys. Rev.* B **77** 224435
[29] Hamer C J, Zheng W H and Singh R R P 2003 *Phys. Rev.* B **68** 214408
[30] Majumdar K 2010 *Phys. Rev.* B **82** 144407
[31] Sushkov O P 2009 *Phys. Rev.* B **79** 174519
[32] Ong A, Uhrig G S and Sushkov O P 2009 *Phys. Rev.* B **80** 014514
[33] Pardini T, Singh R R P, Katanin A and Sushkov O P 2008 *Phys. Rev.* B **78** 024439
[34] Uhrig G S, Holt M, Oitmaa J and Sushkov O P 2009 *Phys. Rev.* B **79** 092416
[35] Bishop R F, Li P H Y, Farnell D J J, Richter J and Campbell C E 2012 *Phys. Rev.* B **85** 205122
[36] Bishop R F and Li P H Y 2011 *Phys. Rev.* A **83** 042111
[37] Farnell D J J, Gernoth K A and Bishop R F 2001 *Phys. Rev.* B **64** 172409